IEEE Access
Multidisciplinary ⋮ Rapid Review ⋮ Open Access Journal

Received January 5, 2022, accepted January 15, 2022, date of publication January 18, 2022, date of current version January 31, 2022.

Digital Object Identifier 10.1109/ACCESS.2022.3144416

Design and Implementation of Ultra-Wide Band Antenna for Partial Discharge Detection in High Voltage Power Equipment

JEAN PIERRE UWIRINGIYIMANA[1], UMAR KHAYAM[1], (Member, IEEE), SUWARNO[1], (Senior Member, IEEE), AND GIAN CARLO MONTANARI[2], (Life Fellow, IEEE)

[1]School of Electrical Engineering and Informatics, Institut Teknologi Bandung, Bandung 40132, Indonesia
[2]Center for Advanced Power Systems, Florida State University, Tallahassee, FL 32306, USA

Corresponding author: Jean Pierre Uwiringiyimana (upeter1@yahoo.fr)

This work was supported in part by the World Class Research Program funded by Kemdikbudristek, Indonesia, and Korea Midland Power Co., Ltd.

ABSTRACT Partial discharges (PD) are the most common and harmful threat to the health of electrical insulation of high voltage (HV) and high field (HF) equipment. The occurrence of PD activity in HV and MV equipment is at the same time a cause and a sign of insulation degradation that may eventually result in the breakdown of the HV power equipment. For the safe and reliable operation of HV power equipment, continuous PD monitoring needs to be conducted conveniently to prevent any unplanned power outages and damage to electrical power equipment. The ultra-high frequency (UHF) PD measurement method has been widely used as an effective technique to detect PD activity on HV power equipment due to its non-invasive principle. To enable PD detection accuracy, there is still a need for more sensitive PD sensors that can assist the UHF PD monitoring system by suppressing ambient background noise and low-frequency electromagnetic interferences from telecommunication such as GSM signals. To tackle the sensitivity issues, this article presents a new design of ultra-wideband (UWB) microstrip patch antenna that is capable of effective suppression of low-frequency interference signals. The proposed antenna, designed, simulated, and optimized using the CST Microwave Studio software, has a bandwidth of 3.3GHz, below -10dB, in the operating frequency range of 1.2GHz-4.5GHz. The prototype of this antenna, printed on an FR4 substrate of a thickness of 1.6mm and a dielectric constant of 4.4, featuring a compact size of 100mm × 100mm × 1.6mm, was implemented to detect PD through laboratory experiments. This paper shows that the designed UWB antenna has high sensitivity, good noise rejection and it is, therefore, a promising candidate sensor for PD detection on HV equipment.

INDEX TERMS Partial discharge, UHF sensors, high-voltage equipment, UWB antenna.

I. INTRODUCTION

Insulation systems play a vital role in the safe delivery of electrical power. However, the failure of insulation may cause the unplanned breakdown of the high voltage (HV) and medium voltage (MV) power equipment, possibly involving explosion and fire that may cause injuries to the people in the vicinity of HV and MV equipment [1], [2]. The Partial discharge phenomenon is one of the extrinsic accelerated aging factors that affect and decrease insulation health and reliability of insulation systems. The presence of PD in insulation stressed by a high electric field (it is field to drive PD rather than voltage) causes local and generally fast insulation degradation to premature breakdown. Partial discharge, according to IEC60270 standards, is a localized electrical discharge that only partially bridges the insulation between conductors and may or may not occur adjacent to a conductor. PD may incept when there is a cavity inside insulation (internal discharge) when there is contamination and/or tangential field gradient on the surface of the insulator (surface discharge) or when there is a protrusion near a high voltage conductor (corona discharges) [3]. When PD incepts in internal cavities or on insulation surface interfaces, the reliability of the insulation system is compromised because the action of PD

The associate editor coordinating the review of this manuscript and approving it for publication was Arpan Kumar Pradhan.

is to break insulating material bonds and disrupt insulation integrity [3], [4]. PD pulses can produce energy in various forms, namely pulsed currents, light, mechanical (acoustic) waves, electromagnetic waves, light and heat that can be detected by various types of sensors [5]. As regards UHF PD sensors, they could be located internally or externally of an HV or MV equipment, being used to detect PD-induced EM waves emitted by PD sources. Typical equipment where UHF PD sensors are used could be power transformer and gas-insulated switchgear, GIS. The advantages of built-in sensors or internal sensors over external sensors are high sensitivity, high signal-to-noise ratio (SNR), and strong immunity to electromagnetic interferences [6]–[8].

The failure or breakdown of key high voltage equipment such as power transformers, gas-insulated switchgears and substation, generators and motors, cables, outdoor insulators and bushings, capacitors may negatively affect the power grid and, in general, electrical assets by causing power outages, loss of equipment, fire explosion and injuries to the people [9]. Partial discharge measurement techniques can be, if properly carried out and analyzed, a fundamental diagnostic tool that contributes to evaluate insulation health conditions. This is then the basis for maintenance action performed at an early stage in order to prevent unwanted outages and blackouts [10], [11].

The ultra-high frequency (UHF) detection method has been widely used for PD detection on high-voltage power apparatus such as switchgears and power transformers, because PD irradiation is, in some equipment, the only way to extract PD information. In addition, the UHF method has high immunity to external electromagnetic interferences [12]–[14]. Noise has, indeed, to be reduced efficiently especially during online (onsite) PD monitoring where there are, e.g., electromagnetic interference from telecommunication, ambient noise and corona discharges [15], [16].

The UHF antenna is an integral part of the UHF PD measurement approach, and it plays a fundamental role in PD detection accuracy, sensitivity and PD localization. Therefore, the design of UHF antennas has gained research and development attention aiming at the improvement of sensitivity and signal-to-noise ratio (SNR). Various UHF antennas have been designed by several researchers. As an example, a planar equiangular spiral antenna, UHF Moore fractal antennas, a dipole antenna and log-periodic antenna are used for GIS [14], [17], [18]. Other types of UHF antennas such as fourth-order Hilbert fractal antennas [16], [12], circular microstrip antenna [19], [20] and microstrip-fed planar elliptical monopole antenna [21] have been designed for PD detection in power transformers.

However, these UHF antennas still face sensitivity challenges due to a narrow bandwidth and a low gain. Therefore, the innovation contribution of the research presented in this paper is about designing an ultra-wideband (UWB) antenna with sufficient bandwidth to detect PD signals with improved sensitivity. A new type of UHF circular microstrip patch antenna with UWB frequency characteristic is proposed here for PD monitoring on HV and MV power equipment. The bandwidth enhancement and a high gain were achieved through the antenna optimization process by using slotting and truncating techniques on the radiating patch and ground plane of the antenna [22]–[24].

This proposed microstrip patch antenna is composed of a radiating patch on one side of an FR4 dielectric substrate and a ground plane on the other side of the substrate. A microstrip feedline was used to connect the patch to a 50 ohm-coaxial cable. The substrate has a dielectric constant of 4.4 and a thickness of 1.6mm. The CST Microwave Studio software was used to design, simulate and optimize the proposed antenna. The optimal design of the microstrip patch antenna has a compact size of 100mm × 100mm × 1.6mm.

After antenna manufacturing, the vector network analyzer, VNA, (Cobalt Series C1220 whose frequency range is 100kHz-20GHz) was used to measure the antenna basic parameters such as return loss, VSWR, resonance frequency, bandwidth and input impedance. The last step was to evaluate the antenna performance for PD detection, as regards sensitivity and noise rejection, through laboratory experiments, which is described in the last section of the paper.

The paper is organized as follows: Section II describes antenna design and simulation, Section III discusses antenna fabrication and testing, Section IV gives the details about antenna validation for PD measurement through laboratory experiments and Section V provides the conclusion highlighting the validity of the research work.

II. ANTENNA DESIGN AND SIMULATION

A. ANTENNA DESIGN CRITERIA

Before designing antennas for PD detection on high voltage power equipment, it is necessary to understand irradiated PD characteristics and frequency spectrum and to relate them to the antenna characteristic parameters in order to meet the desired antenna performance criteria. UHF antennas typically operate in the frequency range of 300MHZ-3GHz, which is the same frequency spectrum for PD-induced EM waves. Indeed, PD pulses may have rise time in the range of (nanoseconds) ns and duration tens to hundreds ns. Based on that, the following antenna basic characteristic parameters need to be tailored when designing UHF antennas able to comply with specified engineering performance criteria.

1) RETURN LOSS

Return loss (RL), in dB, is a logarithmic ratio that compares the reflected power (Pr) of the antenna to the incident power (Pi). Equation (1) provides the relationship between return loss with reflected power and power coming to the antenna.

$$RL = 10\log\left(\frac{P_{reflected}}{P_{incident}}\right) \tag{1}$$

Equation (2) shows the return loss as a function of the reflection coefficient Γ (the ratio of the voltage amplitude of the reflected wave to the voltage amplitude of the incident wave), provided by equation (3). For antenna design criteria,

the return loss value should be at least −10dB within the working frequency range, which means that the reflection coefficient should be at least 0.316.

$$RL = 20\log|\Gamma| \tag{2}$$

$$\Gamma = \frac{V_{reflected}}{V_{incident}} \tag{3}$$

In this condition, the reflected power or power loss back to the source is 10% of the total power delivered to the antenna, while the power received by the antenna is 90%. Therefore, in the antenna design, it is crucial to keep the return loss below −10dB to achieve a good antenna performance.

2) VOLTAGE STANDING WAVE RATIO

Voltage standing wave ratio (VSWR) is a function of the reflection coefficient and it is referred to as the ratio of the maximum voltage amplitude to the minimum voltage amplitude of the standing wave. The standing waves phenomenon occurs when the load (antenna) impedance mismatches with the transmission line impedance (coaxial cable) that feed the antenna. For the ideal antenna, the transmission line impedance or characteristic impedance (Zo = 50ohm) should be equal to the antenna input impedance (Zin). Equations (4) and (5) report the VSWR as a function of maximum and minimum voltages, (4), and the reflection coefficient (5):

$$VSWR = \frac{|V_{\max}|}{|V_{\min}|} \tag{4}$$

$$VSWR = \frac{1+|\Gamma|}{1-|\Gamma|} \tag{5}$$

The VSWR value ranges from 1 to ∞. The closer the VSWR to 1, the better the impedance matching of the antenna and the more power is received. In the antenna design engineering, the allowable VSWR value should be at least equal to 2 throughout the operating frequency band in order to obtain a good impedance matching. It is noteworthy that VSWR = 1 means no power reflected from the antenna, but in practice VSWR > 1 because of some losses that are related to the antenna or transmission line.

3) BANDWIDTH

Absolute bandwidth (ABW) is the difference between the upper and lower frequencies, while fractional bandwidth (FBW) is the percentage of the difference between the highest and lowest frequencies over the center frequency of the bandwidth [25]. Absolute bandwidth and fractional bandwidth can be expressed by equation (6) and equation (7) respectively:

$$ABW = f_H - f_L \tag{6}$$

$$FBW = \frac{f_H - f_L}{f_c} \times 100\% \tag{7}$$

where f_H and f_L indicate the upper and lower cutoff frequencies respectively, while f_c is the center frequency of the frequency band. The bandwidth most properly used is the operating frequency range for which the return loss (RL) value is below −10dB. This shows that the signal power received or transmitted by the antenna reaches 90% of the incoming power.

According to frequency bandwidth, antennas may be classified into three types, namely narrow bandwidth, wide bandwidth and ultra-wide bandwidth. All these types of bandwidths can be used for PD measurement purposes, but narrow bandwidth antenna may cause loss of signal information and signal distortion in the frequency domain. In contrast, the ultra-wideband and broadband antennas are preferred due to their high sensitivity and their ability in capturing PD signals with various frequency components, which will, in turn, helps to analyze the PD severity accurately during data processing [26]. The disadvantage is, in general, the larger sensitivity to noise, thus noise rejection can become an issue to be solved.

4) INPUT IMPEDANCE

The antenna input impedance expressed as Zin is the fundamental parameter for impedance matching. Zin is a function of the reflection coefficient or VSWR. Generally, coaxial cables that are used to connect the designed antennas to the transmission line have a characteristic impedance of 50Ω or 75Ω. Antenna design should be made in a way that the input impedance is equal or very close to the characteristic impedance (Zo) of the coaxial cable. In this case, the return loss due to standing waves is minimized. Equations (8) and (9) can be used to calculate the input impedance of the antenna. The antenna will perfectly match with the transmission line when the reflection coefficient (Γ) close to zero or when the VSWR value is close to one.

$$Zin = Zo \times \frac{1+|\Gamma|}{1-|\Gamma|} \tag{8}$$

$$Zin = Zo \times VSWR \tag{9}$$

B. INITIAL MODEL OF MICROSTRIP PATCH ANTENNA

The initial model is a circular microstrip patch antenna, which can work for PD detection in the UHF range (300MHz-3GHz). This antenna was designed on an FR4 substrate with a dielectric constant of 4.4 (dielectric loss tan $\delta = 0.02$) and a thickness of 1.6mm, with an operating frequency band from 1.2GHz to 3GHz.

The FR4 substrate was chosen in designing this antenna because it is widely used in antenna due to its low cost and its availability on the market. The dielectric constant (relative permittivity) of FR4 substrate is considered to be frequency-dependent at high frequencies, decreasing with the increase of frequency. For the case of FR4, the frequency behavior of the dielectric constant depends on the materials by which it is made (e.g. epoxy resin and glass) [27]. In any case, FR4 has very good performance for UHF frequency band, X-band, and C-band, as reported in the literature [28]–[30].

The size of the initial antenna 100mm × 90mm × 1.6mm (See Fig. 1). The conducting parts of this antenna, namely

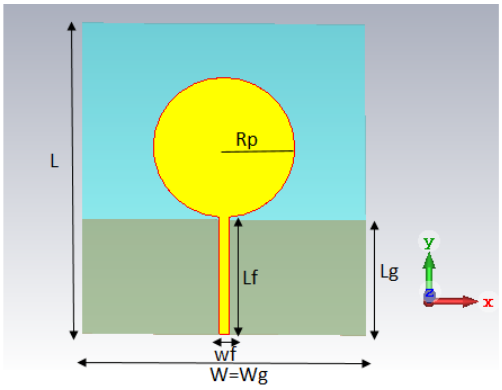

FIGURE 1. Initial model of circular microstrip antenna. Length of the substrate L = 100mm, width of substrate W = 90mm, radius of circular patch Rp = 22.5mm, feedline length Lf = 40mm, feedline width Wf = 1.53m, length of ground plane Lg = 37mm and width of ground plane Wg = 80mm.

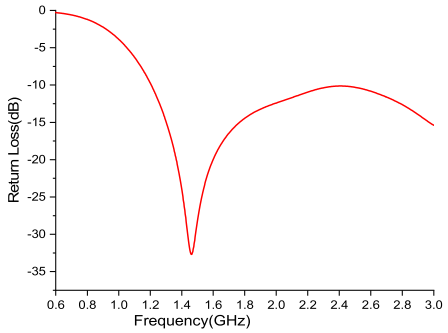

FIGURE 2. Simulated reflection coefficient of the initial model of circular microstrip antenna.

radiating patch and ground plane, are made by annealed copper. The reflection coefficient is plotted as a function of frequency in Fig. 2. This initial antenna design operates in the frequency range of 1.2GHzc-2.4GHz, with a bandwidth of 1200MHz, below −10dB, return loss value −34.5dB at a resonance frequency of 1.45GHz.

C. OPTIMIZATION OF THE MICROSTRIP PATCH ANTENNA

The optimization of the circular microstrip antenna has the purpose to improve ultra-wideband characteristics, which will allow the detection of partial discharge with higher sensitivity by distinguishing the PD signals from unwanted electromagnetic interference signals. The optimization of this antenna was done by modification of the structure of the initial model, truncating the circular patch on its top. In addition, the technique of creating a slot into the ground plane of the antenna was applied to enhance the antenna bandwidth and gain.

Slot techniques have been widely used in telecommunication engineering to improve antenna bandwidth and gain [22]–[24]. The most common slot shapes used in antenna radiating patches or in the ground plane are U-shaped, L-shaped, T-shaped, E-shaped, F-shaped, O-shaped, S-shaped slots, etc [22]. Here, the U-shaped slot on the ground plane is used, with length (Ls), and width (Ws) as depicted in Fig. 3.

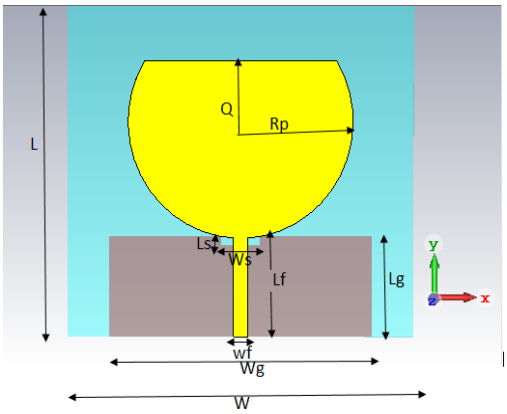

FIGURE 3. Geometrical view of the proposed microstrip antenna, modified with respect to Fig. 1 for the cut of the top of the circular patch and the introduction of the U-shaped slot (antenna dimensions are seen in Table.1).

The U-shaped slot was created in the ground plane of the proposed antenna to widen the bandwidth. According to antenna theory, the existence of the slots in the patch of the antenna or in the ground plane will decrease the quality factor(Q) of the antenna, while the inductance (L) of the antenna will increase, which in turn results in the increase of the bandwidth. Moreover, the presence of the slots in the ground plane or radiating patch will have an effect on the resonance frequency of the antenna when its inductance changes [31].

Equation (10) defines the quality factor of the antenna as the ratio of power stored to the power radiated by the antenna. Equation (11) expresses the resonance frequency as a function of inductance (L) and capacitance (C) of the antenna, which changes with slot creation, and equation (12) gives the quality factor (Q) of the antenna as a function of its inductance. It is seen that when inductance increases, due to the slot, the quality factor (Q) will decrease, which increases the antenna bandwidth (BW) as indicated by equation (13).

$$Q = \frac{P_{stored}}{P_{radiated}} \tag{10}$$

$$f_r = \frac{1}{2\pi\sqrt{LC}} \tag{11}$$

$$Q = \frac{R}{\omega L} \tag{12}$$

$$BW = \frac{1}{Q\sqrt{2}} \tag{13}$$

1) OPTIMIZATION OF PATCH RADIUS

To investigate the effect of the patch radius (Rp) of the antenna on the frequency behavior of the antenna, the size of the patch radius was varied during optimization simulations. The patch radius was 32mm, 32.5mm, 33mm, 33.5, and 34mm. Fig. 4 depicts the simulated S11 parameter or reflection coefficient with various values of patch radius. It is clear that the patch size significantly affects the frequency response of the antenna, as well as the return loss

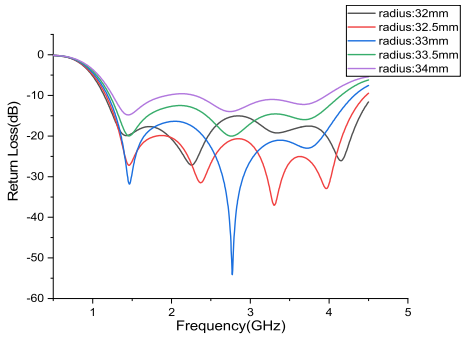

FIGURE 4. Simulated S11 with various values of patch radius.

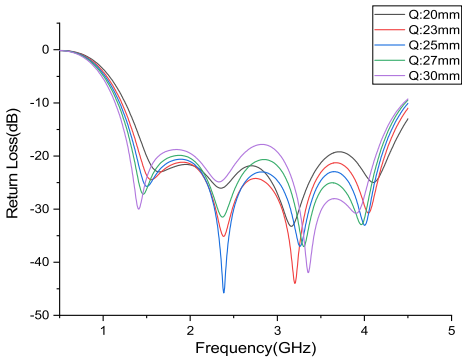

FIGURE 5. Simulated S11 with various sizes of cutting distance.

of the antenna. As an example, an ultra-wideband frequency characteristic of 1.17GHz-4.47GHz can be achieved with lower return loss(under −10dB) in the frequency band of the antenna when a patch radius is 32.5mm, while the bandwidth decreases (e.i,1.4GHz-4.47GHz) and return loss increases when the patch radius is 34mm.

2) CIRCULAR PATCH CUT AND FREQUENCY RESPONSE

The circular patch of the initial antenna model was cut on its top for antenna optimization.

The cutting distance (Q) was varied to investigate its effect on the frequency behavior of the antenna, see Fig. 5. That plots the simulated S11 with different values of the cutting distance. It is observed that an ultra-wideband frequency characteristic with lower return loss was obtained when the cutting distance was 25mm. With this cutting distance, the antenna has a bandwidth of 1.17GHz-449GHz, below −10dB.

3) OPTIMIZATION OF FEEDLINE WIDTH

The feedline width is another antenna parameter that was analyzed to optimize the antenna. Various values of feedline width (Wf) were used to investigate their effect on the frequency characteristic of the antenna, from 3mm to 5 mm, as seen in Fig. 6 to what regards the S11 parameter. It is clear that when the feedline width is 4mm, the UWB frequency characteristic has the lowest return loss at all resonance frequencies throughout the operating frequency band from 1.17GHz to 4.49GHz, under −10dB.

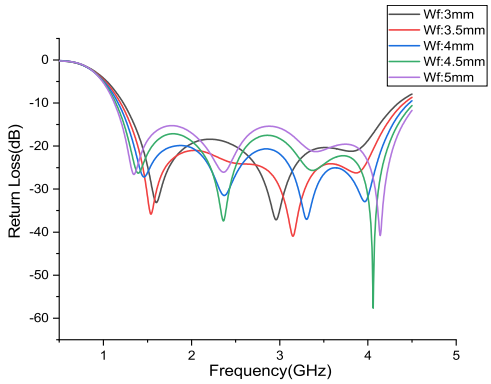

FIGURE 6. Simulated S11 with various size of feedline width.

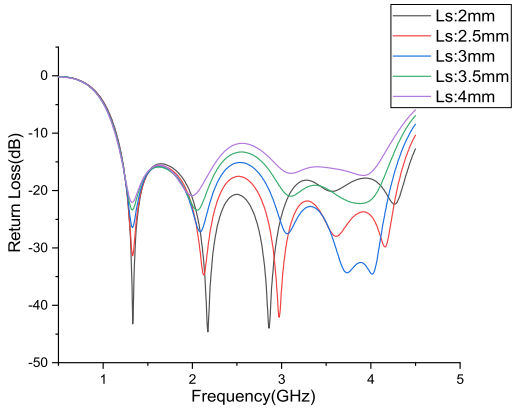

FIGURE 7. Simulated S11 with various size of slot length.

4) OPTIMIZATION OF SLOT LENGTH

The effect of the slot length on the frequency characteristic was investigated by changing slot length (Ls) from 2mm to 4 mm, as seen in Fig. 7. It is seen that using the slot length of 2.5mm, a UWB frequency characteristic was obtained with the lowest return loss within the operating frequency range from 1.12GHz to 4.5GHz, under −10dB.

In the optimization process for the designed antenna, the slot length range of 2mm to 4mm was chosen because it is in this range where the antenna still exhibits a return loss of less than −10dB (in other words, lower reflected power from the antenna back to the source). By choosing the slot length above 4mm or below 2mm, the return loss of the antenna increases, and the voltage standing wave ratio increases too, which will in turn results in poor antenna radiation. According to antenna performance criteria, the return loss should be lower than -10dB and VSWR should be less than 2 within the operating frequency range. In other words, if 100% power is delivered to the antenna, at least 90% of that power will be received by the antenna and 10% of that power will be reflected back to the source as a loss (return loss), as it is expressed by equation (1).

5) OPTIMIZATION OF SLOT WIDTH

Slot width (Ws) was varied from 8mm to 11 mm, being then latter value that provides the minimum S11.

TABLE 1. Optimization parameters for the proposed microstrip antenna.

Parameters		Values
Substrate length	L_p	100mm
Substrate width	W	100mm
Patch radius	Rp	32.5mm
Ground –plane length	Lg	28mm
Ground –plane width	Wg	78mm
Feedline length	Lf	40mm
Feedline width	Wf	4mm
Slot length	Ls	2.5mm
Slot width	Ws	11mm
Substrate permittivity	εr	4.4
Substrate thickness	h	1.6mm

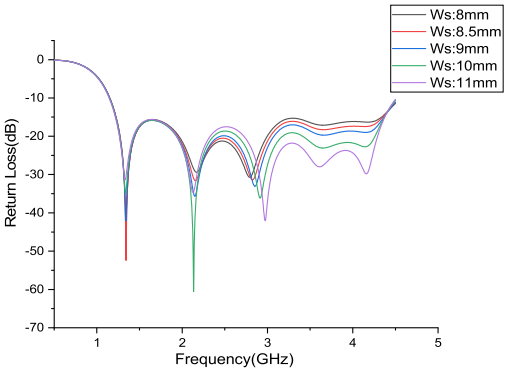

FIGURE 8. Simulated S11 with various size of slot width.

6) SUMMARY OF OPTIMIZATION RESULTS

The results summary of the simulation optimization process is presented in Table 1, which provides the overall dimensions of the optimized antenna.

D. RADIATION PATTERNS OF THE OPTIMIZED ANTENNA

Fig. 9 shows the simulation results of 2-D radiation patterns of the optimized antenna. It is seen that the radiation pattern is almost omnidirectional throughout the entire operating frequency range from 1.12 GHz to 4.5GHz.

The simulation result for the radiation patterns in the E-plane (XY-plane) of the antenna has a dipole-like (eight-shaped) radiation pattern indicating that the maximum antenna radiation is achieved when it is placed vertically to the PD source.

Table 2 shows the simulated maximum gain of the antenna over the entire operating frequency range in both E-plane and H-plane. It is seen that the antenna has a maximum gain in the E-plane than in the H-plane from 1.1GHz-to 3.6GHz. The antenna has a maximum gain in the H-plane than E-plane from 4GHz to 4.5GHz. The average gain value is 2.3dBi in the E-plane and 3.2dBi in the H-plane. This indicates that the designed optimized antenna is potentially capable of detecting PD signals with high sensitivity, since typical antennas used to measure PD signals with a good sensitivity should have an average gain value higher than 2dBi throughout the antenna operating frequency band [19], [21], [32].

The radiation patterns of the designed antenna were simulated for both E-plane and H-plane to analyze the antenna

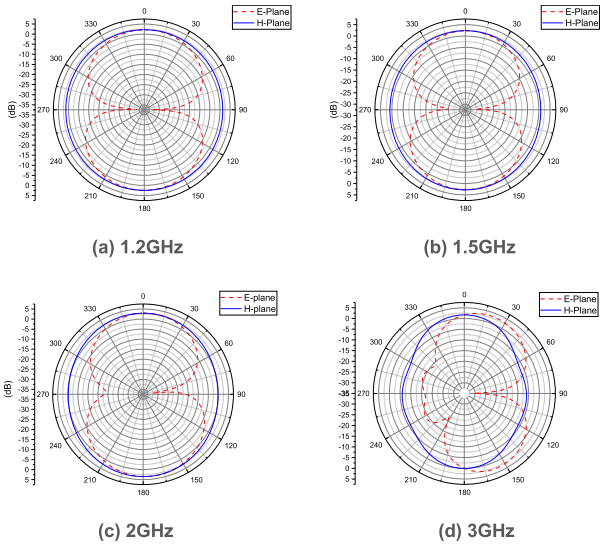

FIGURE 9. Simulated 2D-radiation patterns of the optimized antenna in E-plane and H-plane at: (a) 1.2GHz, (b) 1.5GHz, (c) 2GHz and (d) 3GHz.

radiation patterns, as see in Fig. 9. The E-plane is the plane which contains the electric field vector, while the H-plane is the one that is relevant to the magnetic vector (electromagnetic waves are composed of electric field, E-field, and magnetic field, H-field). The E-plane and H-plane must be 90 degrees apart (since the electric field and magnetic field propagate in the same direction perpendicularly). The direction of maximum radiation may be in either E-plane or H-plane depending upon how the antenna is polarized (either vertically or horizontally) [21]. For our case, the designed antenna has a high gain (higher than 2) in both planes (E-plane and H-plane), indicating how well the antenna is sensitive to PD-induced EM waves.

E. ANALYSIS OF SURFACE CURRENT DISTRIBUTION FOR THE OPTIMIZED ANTENNA

In accordance with the antenna performance theory, the current distribution on the surface of the radiating patch and the surface of the ground plane has a great effect on the antenna sensitivity. Fig. 10 shows the current distribution at a frequency of 2GHz.

It is clear that the maximum current amplitude occurs at the feedline of the antenna, since it connects the antenna to the feed point (excitation port) causing higher concentration of the current on it than in other parts of the antenna. As seen in Fig. 10, a moderate current appears at the surface of the radiating patch and ground plane, decreasing gradually from the feedline, which is common in antenna performance [21],[25]. This conforms that the designed antenna could capture PD-induced EM waves with high sensitivity.

III. ANTENNA FABRICATION AND TESTING

A. FABRICATION OF THE OPTIMIZED ANTENNA

After simulations and relevant optimization, the next step was to fabricate the prototype of the antenna, as shown in Fig. 11.

TABLE 2. Simulated antenna gain over the operating frequency range in E-plane and H-plane.

Frequency(GHz)	Absolute Gain Values(dBi)	
	E-Plane	H-Plane
1.1	2.26	2.26
1.2	2.42	2.42
1.3	2.53	2.53
1.5	2.78	2.78
2	3.54	3.49
2.1	3.7	3.63
2.9	3.25	2.13
3	3.28	1.67
3.6	2.92	2.05
4	1.14	4.82
4.1	0.22	5.2
4.5	-0.067	5.11
Average	**2.33**	**3.17**

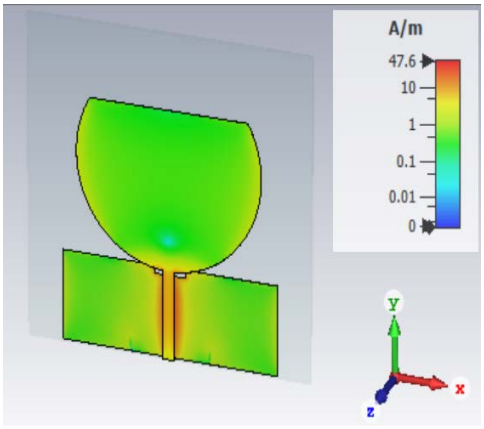

FIGURE 10. Current distribution of the proposed antenna at 2GHz.

This antenna was fabricated on the FR4 substrate printed circuit board (PCB) whose thickness is 1.6mm, dielectric constant = 4.4 and dielectric loss (tan δ) = 0.02. The fabricated antenna has a compact size of 100mm × 100mm × 1.6mm. The radiating patch and ground plane are made of the annealed copper 0.035mm thick.

B. MEASURING THE ANTENNA PARAMETERS USING VECTOR NETWORK ANALYZER

The optimized antenna was tested using a vector network analyzer (VNA) to measure characteristic parameters such as return loss, voltage standing wave ratio (VSWR), bandwidth, resonance frequencies, as seen in Fig. 12. The simulation results were compared to the measurement results obtained by VNA, highlighting that simulation and measurement results are in good agreement.

The slight differences described below between simulation and measurement results might be due to fabrication errors or to the soldering used to link the SMA connector to the feedline of the antenna that was used to link the antenna.

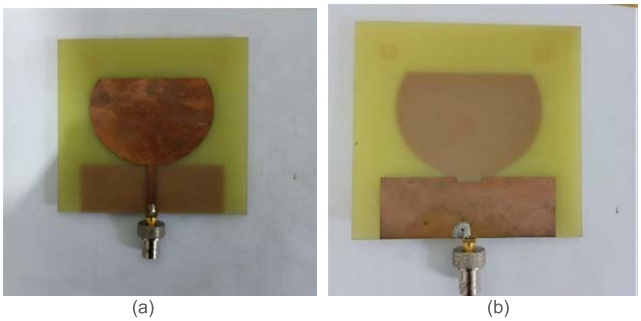

FIGURE 11. Prototype of optimized antenna: (a) Front view showing the radiating patch, (b) back view showing the ground plane.

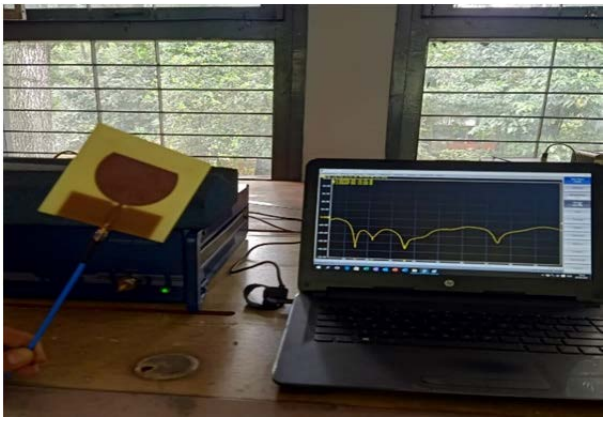

FIGURE 12. Testing the fabricated antenna using the vector network analyzer.

The discrepancy between simulation and measurement results for some parameters could have most likely been caused by fabrication issues or the soldering material used. The additional soldering material (lead) has different characteristics from the copper used on the radiating patch and ground plane of the antenna, which, in turn, may cause the shift in resonance frequencies between the simulation and measurement results of the designed antenna. Indeed, the soldering material was not taken into account in the simulation. The shift in resonance frequencies between simulation and measurement carried out using the vector network analyzer (VNA) is reported and investigated in the recent literature. It is confirmed that the sought cause of discrepancies between simulation and experimental results is related to fabrication and measurement errors [28], [29], [33], [34]. Fig. 12 depicts the antenna testing assembly using the VNA, where the measured frequency response is displayed on the PC screen.

1) MEASUREMENT OF S11 PARAMETER OF THE DESIGNED ANTENNA

Fig. 13 shows the simulated and measured S11 parameter values. Based on the simulation results, the designed antenna has five resonance frequencies, namely 1.3GHz, 2.1GHz, 2.9GHz, 3.6GHz, and 4.1GHz, corresponding to five return loss values of −31.3dB, −34.6dB, −41.8dB, −27.9dB, and −29.3dB respectively. The simulated S11, Fig. 13 a, shows that the antenna has an overall bandwidth of 3.36GHz, below

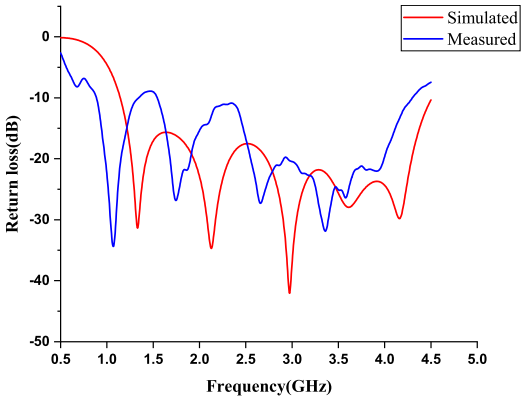

FIGURE 13. Simulated and measured S11 parameters of the designed antenna.

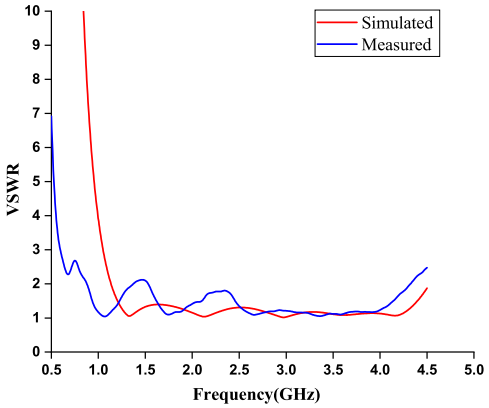

FIGURE 14. Simulated and measured VSWR of the designed antenna.

−10dB over the operating frequency range from 1.14GHz to 4.5GHz.

Based on the measurement results, Fig.13, the manufactured antenna has four resonance frequencies, namely at 1.1GHz, 1.7GHz, 2.5GHz, and 3.4GHz. These resonance frequencies correspond to four return loss values of −35.3dB, −27.6dB, −26.4dB and −31.2dB, respectively. The overall bandwidth of the designed antenna is 3.4GHz, below −10dB over the operating frequency range from 1GHz to 4.4GHz.

2) MEASUREMENT OF VOLTAGE STANDING WAVE RATIO OF THE DESIGNED ANTENNA

The VSWR is an important parameter that indicates how well the radiated waves will propagate through the transmission line (coaxial cable) without being stationary or reflected back to the source. Fig. 14 depicts the simulated and measured VSWR of the designed antenna. Based on the simulation results, it is seen that the values of VSWR for the designed antenna are 1.05, 1.02, 1.03, 1.07, and 1.05, corresponding to five resonance frequencies, namely 1.3GHz, 2.1GHz, 2.9GHz, 3.6GHz, and 4.1GHz, respectively.

Based on the measurement results, the values of VSWR are 1.02, 1.04, 1.05, and 1.03 at four resonance frequencies, namely 1.1GHz, 1.7GHz, and 2.5GHz and 3.4GHz, respectively. It can also be mentioned that the overall VSWR of

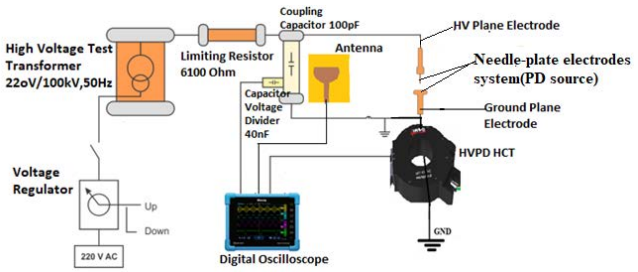

FIGURE 15. Scheme of D measurement circuit components.

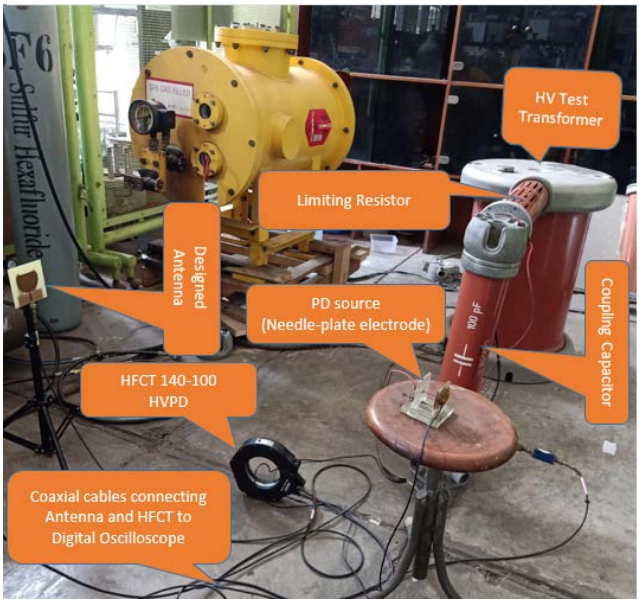

FIGURE 16. Experimental setup for PD measurement with the designed antenna and the commercial HFCT sensor.

the designed antenna from simulation and VNA measurement experiments is less than 2, which, as mentioned, confirms that the designed antenna is suitable for high-sensitivity PD pulse detection. [21].

IV. EXPERIMENTAL VALIDATION

The last step of this research work was to implement the fabricated antenna for PD detection through laboratory experiments. The purpose of these experiments was to verify the sensitivity performance of the designed antenna in detecting PD pulses on the high voltage equipment. In the experiment, a simple needle-plate electrode, test object, was used to generate PD activity in the air (also known as corona discharge).

The gap distance between the tip of the needle electrode and the plate electrode was 10mm. The sensitivity of the designed antenna was investigated by varying the antenna position from the PD source, that is, from 50 cm to 100 cm.

The high voltage supply used in the experiment is a 100 kV, 5 kVA step-up transformer. It feeds the needle-plate electrode (PD source), as seen in Fig.15. A voltage regulator with a range of 0-220 V was used to set the required test voltage (applied voltage), with ratio 1V to 4kV. Two voltage levels, namely 6kV and 7kV, were applied to the test

TABLE 3. Comparison of mean PDIV and mean PD pulse amplitude detected by HFCT and the designed antenna positioned at various positions from PD source.

Sensor	PDIV (kV)	Peak-to-peak Voltage (Vpp) amplitude of the detected PD signal	Positive Peak voltage (Vmax)	Negative peak voltage (Vmin)
Antenna @50cm	3.2kV	35.6mV	23.6mV	-12mV
Antenna @70cm	3.4kV	25.6mV	17.6mV	-8mV
Antenna @100cm	3.6kV	19.2mV	13.2mV	-6mV
HFCT	3.3kV	90mV	50mV	-38mV

object. Fig. 15 shows the PD measurement circuit components, Fig. 16 depicts the experimental setup for PD measurement using the designed antenna and the commercial high frequency current transformer (HFCT 140-100 HVPD) sensor connected to the ground lead. The purpose of using HFCT was to compare and validate the antenna performance. Antenna and HFCT sensors were connected to a digital oscilloscope using a 50-Ohm coaxial cable.

To carry out PD measurement experiment, 20 data samples were taken for each applied voltage and for each antenna position. Then, the average peak-to-peak voltage (Vpp) of the detected PD signal waveforms were calculated during the PD data processing.

Electromagnetic waves emitted by PD activity on high voltage equipment can be affected by electromagnetic interferences present in the experimental environment. According to IEC60270 standard, it is advised to conduct the PD measurement when there is a low level of noise in the measurement environment to be able to detect PD activity with higher sensitivity and accuracy [35]. Before carrying out the PD measurement experiments in our laboratory, the background noise was measured before and after switching on the test voltage source. In the latter case, the average peak-to-peak voltage (Vpp) amplitude of the background noise measured by antenna and HFCT were 6mV and 6.6 mV, respectively. Then the applied voltage was increased gradually until the first PD pulse signals occurred (known as partial discharge inception voltage, PDIV). Based on signal shape, PD pulses were separated from noise using visual evaluation and wavelet tools [36], [37].

After assessing the background noise, the next step was to measure the partial discharge inception voltage (PDIV) for the designed antenna and HFCT.

Table 3 summarizes mean PDIV and PD pulse signals detected by the designed antenna positioned at 50cm, 70cm, and 100cm from the PD source. It is observed that the antenna positioned at a distance of 50cm from the PD source will detect PD pulse signals at an inception voltage of 3.2kV with mean pulse amplitude of 35.6mV, being more sensitive than

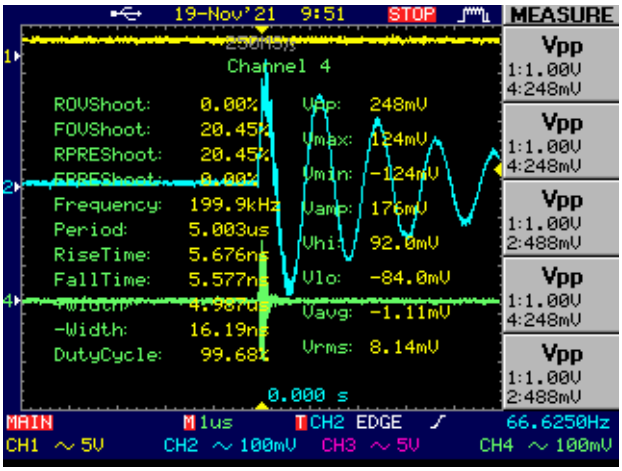

FIGURE 17. A typical PD signal waveform detected by the antenna placed at 100cm from the PD source simultaneously with the HFCT sensor when the applied voltage was 7kV.

the antenna placed farther from the PD source. In other words, the PDIV slightly increases with the increase of the distance between the antenna and the PD source, and the amplitude of the detected PD pulses at PDIV decreases with the increase of the distance between the antenna and the PD source.

Table 3 also indicates that the PDIV for HFCT is comparable with that obtained by the antenna positioned at a distance of 50 cm to 70 cm from the PD source, even if the sensitivity of the former is larger than that of the latter (higher PD pulse magnitude).

Fig. 17 shows the oscilloscope display for the typical waveforms of the PD signals detected by the designed antenna and, simultaneously, by the commercial HFCT, used as a reference sensor, when the applied test voltage was 7kV and when the antenna was positioned100cm away from the PD source. The HFCT was connected to channel 2 (CH2) while the antenna was connected to channel 4(CH4), and the source voltage was connected to channel 1 (CH1) on the oscilloscope.

Fig. 18 to Fig. 20 depict the time-domain PD signal waveforms detected by using the designed antenna and the commercial HFCT sensor at 6kV and 7kV when the antenna was positioned at a distance of 50 cm, 70 cm, and 100 cm from the PD source, respectively.

Table 4 represents a summary of PD measurement results obtained by using the designed antenna and the commercial HFCT sensor. Based on these measurement results, it can be argued that the designed antenna is able to detect EM waves emitted by PD activity in high and medium voltage equipment. The designed antenna has highest sensitivity when it is placed at less than 50cm from the PD source, but it can still have good sensitivity when placed even at a distance of 1m from the PD source. It can be mentioned that the HFCT was only used as a comparison sensor to validate the acquisition capability and the relevant PD waveforms detected by the designed antenna. The shape and amplitude of the detected PD signal between antenna and HFCT are different because the mode of detection also differs. Indeed, the HFCT sensor

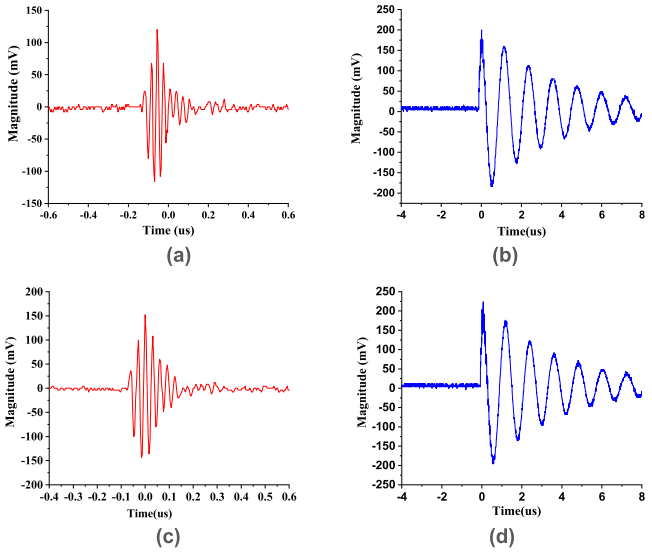

FIGURE 18. PD signals waveforms detected by the designed antenna and the HFCT when the antenna was positioned at 50 cm from PD source: (a) antenna at 6kV, (b) HFCT at 6kV, (c) antenna at 7kV and (d) HFCT at 7kV.

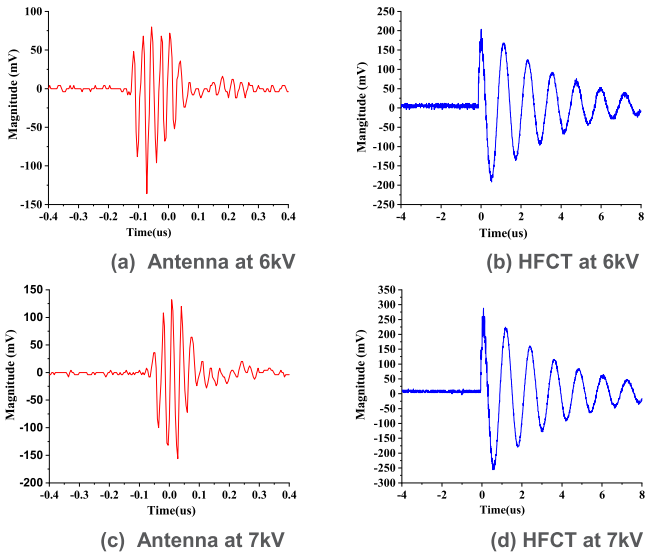

FIGURE 19. PD signals waveforms detected by the designed antenna and the HFCT when the antenna was positioned at 70 cm from PD source: (a) antenna at 6kV, (b) HFCT at 6kV, (c) antenna at 7kV and (d) HFCT at 7kV.

detects the PD impulse current flowing to the ground wire while the antenna detects EM emitted by PD activity.

Eventually, the optimized antenna was compared with the initial antenna in detecting PD signals to investigate how much sensitivity was improved. Fig. 21 (a) and (b) show an example of sensitivity comparison between the initial antenna and optimized antenna when both antennas were positioned at a distance of 70cm from the PD source and when the applied voltage was 6kV and 7kV, respectively.

As can be seen, at 6 kV the peak-to-peak voltage of the UHF PD signal detected by the initial antenna and optimized antenna are 98mV and 216mV, respectively while at 7kVthe difference is 122mV and 296mV. This indicates that the

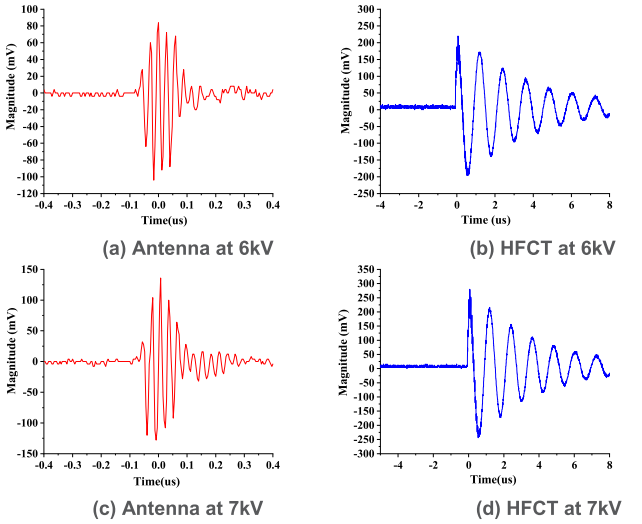

FIGURE 20. PD signals waveforms detected by the designed antenna positioned and the HFCT when the antenna was at 100 cm from PD source: (a) antenna at 6kV, (b) HFCT at 6kV, (c) antenna at 7kV and (d) HFCT at 7kV.

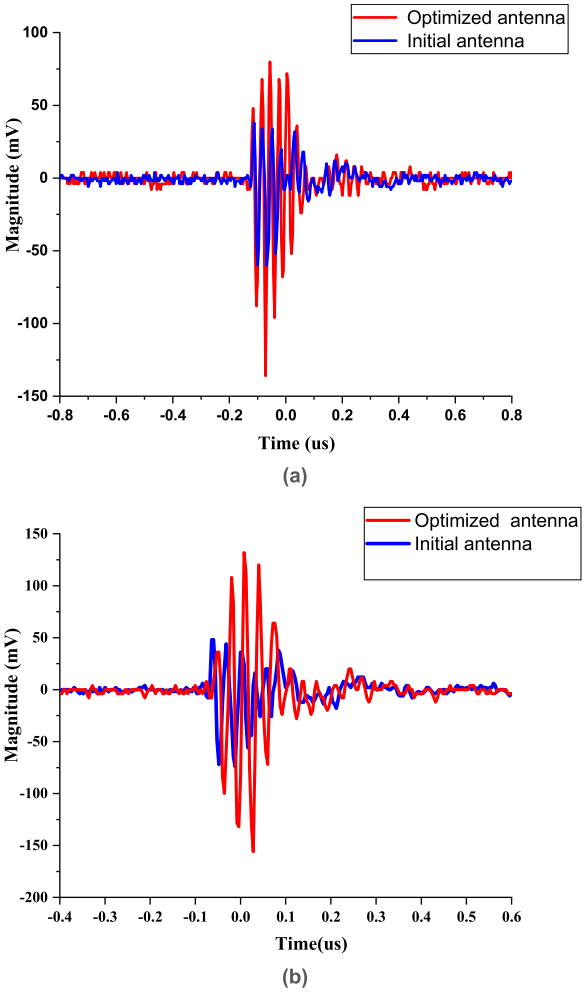

FIGURE 21. UHF PD signals detected by initial antenna and optimized antenna at a distance of 70 cm from PD source: (a) at 6kV and (b) at 7kV.

optimized antenna is roughly twice more sensitive than the initial antenna.

TABLE 4. PD signal magnitude detected by the designed antenna at various positions in comparison with commercial HFCT at 6kV and 7kV.

Sensor position from PD source	Antenna		HFCT	
	Applied voltage		Applied voltage	
	6kV	7kV	6kV	7kV
	Peak-to-peak voltage of detected PD signal(mV)	Peak-to-peak voltage of detected PD signal(mV)	Peak-to-peak voltage of detected PD signal(mV)	Peak-to-peak voltage of detected PD signal(mV)
50cm	236	296	384	420
70cm	216	288	396	544
100cm	188	264	416	524

V. CONCLUSION

This paper deals with the optimized design and validation of a UWB antenna that can be used for partial discharge monitoring on high and medium-voltage power equipment. The antenna is designed to have an ultra-wide bandwidth in the frequency range of 1.1GHz to 4.4GHz, which prompts high sensitivity by attenuating the low-frequency ambient noise that may interfere with PD signals. As depicted in Fig. 17, the background noise detected by the designed antenna was only 6mV while the peak-to-peak voltage (Vpp) of the PD signal detected by the antenna is 248mV.

The simulation results of the designed antenna are in good agreement with the measurement results obtained by using the vector network analyzer. The slight difference should be related to fabrication issues and/or to the soldering material used to link the feedline of the antenna with the SMA connector that joins the antenna to the coaxial cable.

Based on the measurement results, the designed antenna has a low return loss(less than −10dB) and a VSWR close to 1 at all resonance frequencies of the antenna.

To investigate the sensitivity performance, the antenna was used to detect PD signals through laboratory experiments. The antenna sensitivity was verified by varying its position from the PD source. In addition, the PD measurement results provided by the designed antenna were compared with those obtained by the initial, not optimized, antenna and a commercial HFCT sensor. In this way, it has been highlighted that the optimized antenna has higher sensitivity than the initial antenna in detecting EM waves emitted by PD activity, but it shows lower sensitivity than the HFCT. However, the PDIV measured by the optimized antenna and that from the HFCT are relatively very close as long as the antenna is not farer than about 70 cm from the test object.

To conclude, the proposed antenna is a suitable and promising candidate PD sensor that can assist UHF PD monitoring of high and medium voltage power apparatuses, where irradiated UHF PD signals can be potentially sensed.

REFERENCES

[1] J. P. Uwiringiyimana and U. Khayam, "Measurement of partial discharge in air insulation by using UHF double layer bowtie antenna with modified wings edges," in *Proc. Int. Conf. Electr. Eng. Informat. (ICEEI)*, Jul. 2019, pp. 228–233.

[2] J. P. Uwiringiyimana and U. Khayam, "Design and application of double layer bowtie antenna and single layer bowtie antenna as UHF sensors for partial discharge detection," *IOP Conf. Ser., Mater. Sci. Eng.*, vol. 850, no. 1, May 2020, Art. no. 012036.

[3] S. Suwarno, "Partial discharge in high voltage insulating materials," *Int. J. Electr. Eng. Informat.*, vol. 8, no. 1, pp. 147–163, Mar. 2016.

[4] U. Khayam and F. I. Fatoni, "Design and application of loop antenna for partial discharge induced electromagnetic wave detection," in *Proc. 6th Int. Conf. Electr. Eng. Informat. (ICEEI)*, Nov. 2017, pp. 1–6.

[5] F. Rozi and U. Khayam, "Development of loop antennas for partial discharge detection," *Int. J. Electr. Eng. Informat.*, vol. 7, no. 1, pp. 29–41, Mar. 2015.

[6] D.-S. Kim, C.-M. Hwang, Y.-N. Kim, J.-O. Choi, W.-B. Seo, B.-S. Han, S.-H. Choi, and Y.-M. Jang, "Development of an intelligent spacer built into the internal-type UHF partial discharge sensor," in *Proc. Conf. Rec. IEEE Int. Symp. Electr. Insul.*, Jun. 2008, pp. 396–399.

[7] M. D. Judd, "Experience with UHF partial discharge detection and location in power transformers," in *Proc. Electr. Insul. Conf. (EIC)*, Jun. 2011, pp. 201–205.

[8] S.-G. Ha, J. Cho, J. Lee, B.-W. Min, J. Choi, and K.-Y. Jung, "Numerical study of estimating the arrival time of UHF signals for partial discharge localization in a power transformer," *J. Electromagn. Eng. Sci.*, vol. 18, no. 2, pp. 94–100, Apr. 2018.

[9] L. Luo, B. Han, J. Chen, G. Sheng, and X. Jiang, "Partial discharge detection and recognition in random matrix theory paradigm," *IEEE Access*, vol. 5, pp. 8205–8213, 2016.

[10] B. Sheng, C. Zhou, D. M. Hepburn, X. Dong, G. Peers, W. Zhou, and Z. Tang, "Partial discharge pulse propagation in power cable and partial discharge monitoring system," *IEEE Trans. Dielectr. Electr. Insul.*, vol. 21, no. 3, pp. 948–956, Jun. 2014.

[11] P. Li, W. Zhou, S. Yang, Y. Liu, Y. Tian, and Y. Wang, "Method for partial discharge localisation in air-insulated substations," *IET Sci., Meas. Technol.*, vol. 11, no. 3, pp. 331–338, Jan. 2017.

[12] J. Lopez-Roldan, T. Tang, and M. Gaskin, "Optimisation of a sensor for onsite detection of partial discharges in power transformers by the UHF method," *IEEE Trans. Dielectr. Electr. Insul.*, vol. 15, no. 6, pp. 1634–1639, Dec. 2008.

[13] M. Siegel, M. Beltle, S. Tenbohlen, and S. Coenen, "Application of UHF sensors for PD measurement at power transformers," *IEEE Trans. Dielectr. Electr. Insul.*, vol. 24, no. 1, pp. 331–339, Feb. 2017.

[14] T. Li, M. Rong, C. Zheng, and X. Wang, "Development simulation and experiment study on UHF partial discharge sensor in GIS," *IEEE Trans. Dielectr. Electr. Insul.*, vol. 19, no. 4, pp. 1421–1430, Aug. 2012.

[15] R. Bell, C. Charlson, S. P. Halliday, T. Irwin, J. Lopez-Roldan, and J. Nixon, "High-voltage onsite commissioning tests for gas-insulated substations using UHF partial discharge detection," *IEEE Trans. Power Del.*, vol. 18, no. 4, pp. 1187–1191, Oct. 2003.

[16] A. A. Zahed, A. H. El-Hag, N. Qaddoumi, R. Hussein, and K. B. Shaban, "Comparison of different fourth order Hilbert fractal antennas for partial discharge measurement," *IEEE Trans. Dielectr. Electr. Insul.*, vol. 24, no. 1, pp. 175–182, Feb. 2017.

[17] Y. Wang, Z. Wang, and J. Li, "UHF Moore fractal antennas for online GIS PD detection," *IEEE Antennas Wireless Propag. Lett.*, vol. 16, pp. 852–855, 2016.

[18] J. Ardila-Rey, J. Martínez-Tarifa, G. Robles, and M. V. Rojas-Moreno, "Partial discharge and noise separation by means of spectral-power clustering techniques," *IEEE Trans. Dielectr. Electr. Insul.*, vol. 20, no. 4, pp. 1436–1443, Aug. 2013.

[19] G. V. R. Xavier, A. J. R. Serres, E. G. da Costa, and C. C. R. de Albuquerque, "Circular printed monopole antenna with slotted ground plane for application in the detection of partial discharges in power transformers," in *Proc. 4th Int. Symp. Instrum. Syst., Circuits Transducers (INSCIT)*, Aug. 2019, pp. 1–5.

[20] G. V. R. Xavier, E. G. Da Costa, A. J. R. Serres, H. F. S. Sousa, A. C. D. Oliveira, and L. A. M. M. Nobrega, "Design and application of an UHF microstrip circular antenna for partial discharges detection in power transformers," in *Proc. ICHVE IEEE Int. Conf. High Volt. Eng. Appl.*, Sep. 2019, pp. 2–5.

[21] H. Chai, B. T. Phung, and D. Zhang, "Development of UHF sensors for partial discharge detection in power transformer," in *Proc. Condition Monitor. Diagnosis (CMD)*, Sep. 2018, pp. 1–5.
[22] P. P. Chandran and S. Viswasom, "Gain and bandwidth optimization of a novel microstrip patch antenna," in *Proc. 4th Int. Conf. Adv. Comput. Commun.*, Aug. 2014, pp. 315–318.
[23] J.-S. Kuo and G.-B. Hsieh, "Gain enhancement of a circularly polarized equilateral-triangular microstrip antenna with a slotted ground plane," *IEEE Trans. Antennas Propag.*, vol. 51, no. 7, pp. 1652–1656, Jul. 2003.
[24] Y. Rahayu, T. A. Rahman, R. Ngah, and P. S. Hall, "Slotted ultra wideband antenna for bandwidth enhancement," in *Proc. Loughborough Antennas Propag. Conf.*, Mar. 2008, pp. 449–452.
[25] C. A. Balanis, "Antenna theory: Analysis and design," Tech. Rep., 2012.
[26] H. H. Sinaga, B. T. Phung, and T. R. Blackburn, "Partial discharge localization in transformers using UHF detection method," *IEEE Trans. Dielectr. Electr. Insul.*, vol. 19, no. 6, pp. 1891–1900, Dec. 2012.
[27] S. J. Mumby and J. Yuan, "Dielectric properties of FR-4 laminates as a function of thickness and the electrical frequency of the measurement," *J. Electron. Mater.*, vol. 18, no. 2, pp. 287–292, Mar. 1989.
[28] Y. Qi, Y. Fan, G. Bing, R. Jia, W. Sen, S. Wei, and A. Jadoon, "Design of ultra-wide band metal-mountable antenna for UHF partial discharge detection," *IEEE Access*, vol. 7, pp. 60163–60170, 2019.
[29] S. Park and K. Y. Jung, "Design of a circularly-polarized uhf antenna for partial discharge detection," *IEEE Access*, vol. 8, pp. 81644–81650, 2020.
[30] A. A. Qureshi, M. U. Afzal, T. Taqueer, and M. A. Tarar, "Performance analysis of FR-4 substrate for high frequency microstrip antennas," in *Proc. China-Japan Jt. Microw. Conf. (CJMW)*, Jul. 2017, pp. 159–162.
[31] A. Munir, G. Petrus, and H. Nusantara, "Multiple slots technique for bandwidth enhancement of microstrip rectangular patch antenna," in *Proc. Int. Conf. QiR*, Jun. 2013, pp. 150–154.
[32] S. M. Mukhtar, M. Isa, and A. A. Al-Hadi, "Design of UHF antenna sensor for partial discharge detection in high voltage S ubstation," *IOP Conf. Ser. Mater. Sci. Eng.*, vol. 318, no. 1, 2018, Art. no. 012052.
[33] Z. Cui, S. Park, H. Choo, and K.-Y. Jung, "Wideband UHF antenna for partial discharge detection," *Appl. Sci.*, vol. 10, no. 5, p. 1698, Mar. 2020.
[34] L. A. M. M. Nobrega, G. V. R. Xavier, M. V. D. Aquino, A. J. R. Serres, C. C. R. Albuquerque, and E. G. Costa, "Design and development of a bio-inspired UHF sensor for partial discharge detection in power transformers," *Sensors*, vol. 19, no. 3, pp. 1–16, 2019.
[35] C. Ma, H. Li, W. Zhou, J. Yu, L. Wang, S. Yang, and S. Hu, "Background noise of partial discharge detection and its suppression in complex electromagnetic environment," in *Proc. IEEE Int. Conf. High Voltage Eng. Appl. (ICHVE)*, Sep. 2018, pp. 1–4.
[36] J. P. Uwiringiyimana and U. Khayam, "Noise measurement in high voltage laboratory by using high frequency current transformer and loop antenna," in *Proc. Int. Conf. High Voltage Eng. Power Syst. (ICHVEPS)*, Oct. 2017, pp. 35–39.
[37] H. Zhang, T. R. Blackburn, B. T. Phung, and D. Sen, "A novel wavelet transform technique for on-line partial discharge measurements. 2. on-site noise rejection application," *IEEE Trans. Dielectr. Electr. Insul.*, vol. 14, no. 1, pp. 15–22, Feb. 2007.

JEAN PIERRE UWIRINGIYIMANA received the B.Sc. degree in electrical engineering from the National University of Rwanda, Rwanda, in 2013, and the M.Sc. degree in electrical engineering from the Institut Teknologi Bandung, Bandung, Indonesia, in 2019, where he is currently pursuing the Ph.D. degree in electrical engineering. He has published several conference papers and journal articles in the field of high voltage engineering. His current research interests include partial discharge diagnosis on high voltage power apparatuses, development of UHF sensors for partial discharge monitoring on high voltage power apparatuses, and condition monitoring of high voltage power equipment based on partial discharge measurement technique.

UMAR KHAYAM (Member, IEEE) received the B.Sc. and M.Sc. degrees from the Department of Electrical Engineering, Institut Teknologi Bandung (ITB), Indonesia, in 1998 and 2000, respectively, and the Ph.D. degree from the Kyushu Institute of Technology, Japan, in 2005. He is currently an Associate Professor with the Power Engineering Research Group, School of Electrical Engineering and Informatics, ITB. He is also the Head of the High Voltage and High Current Engineering Laboratory and the Head of the Doctoral Study Program of Electrical Engineering and Informatics, ITB. He has published more than 140 international conference papers and journal articles. His research interests include high voltage engineering, mainly on the development of diagnosis system of power apparatus based on partial discharge measurement technique. He received the best paper award from few international conferences, in 2005, 2014, 2016, and 2018.

SUWARNO (Senior Member, IEEE) received the B.Sc. and M.Sc. degrees from the Department of Electrical Engineering, Institut Teknologi Bandung, Indonesia, in 1988 and 1991, respectively, and the Ph.D. degree from Nagoya University, Japan, in 1996. He is currently a Professor and the Emeritus Dean of the School of Electrical Engineering and Informatics, Institut Teknologi Bandung. He is serving as the Head for the Electrical Power Engineering Research Group, School of Electrical Engineering and Informatics, ITB. He has published over 260 international journal and conference papers. His research interests include high voltage insulating materials, technology, and diagnostics of HV equipment. He received the Student Best Awards from IEEJ, Japan, in 1994 and 1995; IEEE Queensland, Australia, in 1994; and ACED, Seoul, South Korea, in 2002. He was elected as the First Winner of Outstanding Indonesian Lecturers by the Ministry of Education and Culture, in 2009. He was the General Chairperson of several IEEE sponsored international conferences, such as ICPADM 2006, ICEEI 2007, CMD 2012, ICHVEPS 2017, ICHVEPS 2019, and ICHVEPS 2021. He has been listed in top 2% of the world's most influential scientists according to a study conducted by Stanford University, in 2021. He is the Editor-in-Chief for the *International Journal on Electrical Engineering and Informatics*.

GIAN CARLO MONTANARI (Life Fellow, IEEE) is currently a Research Faculty III at the Center for Advanced Power Systems (CAPS), Florida State University, USA; an Alma Mater Professor at Bologna University, Italy; and an Adjunct Professor at Bandung University, Indonesia. He has been a Full Professor of electrical technology at the Department of Electrical, Electronic and Information Engineering, University of Bologna, teaching courses on electrical technology, reliability, and asset management. Since 1979, he has working in the field of aging and endurance of insulating materials and systems, diagnostics of electrical systems, asset management, and innovative electrical materials (magnetics, electrets, super-conductors, and nano-materials). He has also been engaged in the fields of power quality and energy market, power electronics, reliability and statistics of electrical systems, and smart grid. He was the Founder and the President of the spin-off Techimp, established, in 1999. He is the author or the coauthor of more than 800 scientific papers. He has been recognized with several awards, including the IEEE Ziu-Yeda, Thomas W. Dakin, Whitehead, Eric Forster, and IEC 1906 Awards.